The X-ray Spectra of Black Hole X-ray Novae in Quiescence as Measured by *Chandra*

Albert K.H. Kong, Jeffrey E. McClintock, Michael R. Garcia, Stephen S. Murray

Harvard-Smithsonian Center for Astrophysics, 60 Garden Street, Cambridge, MA 02138

Didier Barret

Centre d'Etude Spatiale des Rayonnements, 9 Avenue du Colonel Roche, 31028 Toulouse, France

ABSTRACT

We present *Chandra* observations of black hole X-ray novae V404 Cyg, A0620–00, GRO J1655–40 and XTE J1550–564 in quiescence. Their quiescent spectra can be well fitted by a power-law model with number slope $\alpha \sim 2$. While a coronal (Raymond-Smith) model is also a statistically acceptable representation of the spectra, the best fit temperatures of these models is ~ 5 times higher than that seen in active stellar coronae. These four spectra of quiescent X-ray novae are all consistent with that expected for accretion via an advection-dominated accretion flow (ADAF) and inconsistent with that expected from a stellar corona. This evidence for continued accretion in quiescence further strengthens the case for the existence of event horizons in black holes. Both A0620–00 and GRO J1655–40 were fainter than in previous observations, while V404 Cyg was more luminous and varied by a factor of 2 in a few ksec. A reanalysis of the X-ray data for XTE J1550–564 shows that (like V404 Cyg and A0620–00) its luminosity exceeds the maximum prediction of the coronal model by a large factor. The 0.3–7 keV luminosity of the four sources studied ranges from $\sim 10^{30} - 10^{33}$ erg s^{-1}.

Subject headings: binaries: close — black hole physics — stars: individual (V404 Cyg, A0620–00, GRO J1655–40, XTE J1550–564) — X-rays: stars

1. Introduction

X-ray Novae (XN) are compact binary systems in which a Roche-lobe-overflowing main sequence or subgiant star, typically $\sim 1\,M_\odot$, transfers matter onto a black hole (BH) or neutron star (NS) primary (for a review, see van Paradijs & McClintock 1995; Tanaka & Lewin 1995; Tanaka & Shibazaki 1996). XN are highly variable and undergo rare but dramatic X-ray and optical outbursts. For most of the time, XN are in a quiescent state and are very faint. During quiescence, the mass accretion rate from the disk to the compact object may be very small, producing a low level (perhaps no) X-ray emission. X-ray observations of quiescent XN have been hindered due to the limited sensitivity of previous X-ray telescopes. Nonetheless, several of the brightest black hole X-ray novae (BHXN) have been detected with *ROSAT*, *ASCA* and *BeppoSAX*. This quiescent X-ray (and associated non-stellar optical) emission is difficult to explain using standard accretion disk models. Narayan, McClintock, & Yi (1996), Narayan, Barret, & McClintock (1997a) and Narayan, Garcia, & McClintock (2001) showed that the observations can be explained by an advection-dominated accretion flow (ADAF) model.

An ADAF is an accretion flow in which most of the energy is stored in the accreting gas rather than being radiated away promptly, as in a thin accretion disk. This thermal energy is advected with the flow to the center – hence the name ADAF. If the accretor is a BH, the gas with all its thermal energy will be lost from view as it falls through the event horizon. However, in the case of a NS, the accretion energy will eventually be radiated from the star's surface. This difference can explain the fact that quiescent BHs are much fainter than quiescent NSs. Using pre-*Chandra* data, Narayan, Garcia, & McClintock (1997b) showed that BHs display a large variation of luminosity between their bright and their faint states, while NSs have a much smaller variation. Menou et al. (1999) subsequently pointed out that in comparing the luminosities of BH and NS systems, it is important to compare systems with comparable orbital periods. More recently, Garcia et al. (2001; hereafter G01) presented a comprehensive study of a series of *Chandra* observations of BHXN in quiescence; they confirmed that the quiescent X-ray luminosities of BHXN are ~ 100 lower than those of neutron star X-ray novae (NSXN). Such findings provide strong evidence that BHs have event horizons.

Recently, Bildsten & Rutledge (2000) suggested that the rapidly rotating secondaries of BHXN may generate stellar coronae with sufficient X-ray luminosity to account for the observed quiescent luminosities of many of these systems. Based on an analogy to the 'saturated' coronae in the most luminous RS CVn stars, the coronae in quiescent BHXN are predicted to have maximum luminosities of 0.1% of the stellar bolometric luminosity, and X-ray spectra that are typical of moderately hot ($kT \lesssim 1$ keV), optically thin thermal plasmas. While the X-ray luminosity of V404 Cyg is too high to be produced by a stellar corona, previous observations with modest sensitivity have indicated that the luminosities of other BHXN are consistent with a saturated corona (Bildsten & Rutledge 2000). For these systems, the high S/N X-ray spectra attainable with *Chandra* and *XMM-Newton* can provide a critical test of the possible coronal origin of the quiescent X-ray luminosity (Bildsten & Rutledge 2000; Lasota 2001).

In this paper, we report the detailed analysis of *Chandra* spectra of the brightest three quiescent BHXN observed under an AO-1 GTO program (V404 Cyg, A0620–00 and GRO J1655–40). We also reanalyzed the spectrum of a fourth BHXN (XTE J1550–564) observed under a DDT proposal. We note that three other BHXN (GRO J0422+32, GS 2000+25 and 4U 1543–47) observed under our AO-1 GTO and GO programs provided insufficient counts for spectral analysis. We briefly describe previous quiescent observations of these four sources in § 2. In § 3 we outline our analysis procedure and report the results in § 4. The results are discussed in § 5.

2. Previous Quiescent X-ray Observations

All four BHXN have been observed previously in the X-ray, and a summary of previous quiescent observations is given in Table 1; we here discuss them briefly.

V404 Cyg — This relatively bright quiescent BHXN has previously been observed by *ROSAT*, *ASCA* and *BeppoSAX* (see Table 1). In general, the X-ray spectrum can be fitted by a power-law model with photon index $\alpha \sim 2$ and $N_H \sim (1-2) \times 10^{22}$ cm^{-2}; the luminosity is $\sim 10^{33}$ ergs s^{-1} (Narayan et al. 1997a). We also note that the quiescent source flux can vary on short time scales. Wagner et al. (1994) reported that V404 Cyg decreased in intensity by a factor of 10 in < 0.5 day and showed variability by a factor of ~ 2 on time scales of ~ 30 minutes.

A0620–00 — This source was observed by *ROSAT* in 1992 during its quiescent state (McClintock et al. 1995; Narayan et al. 1997a). The 39 ± 8 counts detected allowed only a modest estimate of the source spectrum. Simple one component models fit the spectrum equally well: for example a power-law with $\alpha \sim 3.5$ and $N_H = (0.1-1) \times 10^{22}$ cm^{-2} or a blackbody with $kT = 0.16^{+0.10}_{-0.05}$ keV. The luminosity is $\sim 5 \times 10^{30}$ ergs s^{-1}. An *ASCA* observation in 1994 March failed to detect the source; a 3σ upper limit on the luminosity was 8×10^{30} ergs s^{-1} (Asai et al. 1998).

GRO J1655–40 — The only quiescent observation of GRO J1655–40 was taken in 1996 March with *ASCA* (Ueda et al. 1998; Asai et al. 1998). The spectrum can be fitted by a power-law model with a photon index $\alpha \sim 0.7$ and $N_H < 3 \times 10^{21}$ cm^{-2}; the source luminosity is 3×10^{32} ergs s^{-1} in 0.5–10 keV. However, we note that this observation was taken between two outbursts separated by ~ 1 years and therefore it may not represent the true quiescent emission.

XTE J1550–564 — This microquasar system was observed as a DDT program on 2000 August 21 and 2000 September 11, which were > 120 d after the peak of the 2000 outburst of the source; a detailed spectral analysis has already been given by Tomsick, Corbel, & Kaaret (2001). The energy spectrum can be fitted by an absorbed power-law spectrum with $\alpha = 2.3^{+0.41}_{-0.48}$ and $N_H = (8.5^{+2.2}_{-2.4}) \times 10^{21}$ cm^{-2}; the mean luminosity (0.5–7 keV) is about 6.7×10^{32} erg s^{-1}.

3. Chandra Observations and Data Reduction

V404 Cyg — *Chandra* observed V404 Cyg on 2000 April 26 for a total of 10,295 s. Our observations cover spectroscopic phases 0.44–0.46 (Casares & Charles 1994), where phase zero corresponds to the closest approach of the secondary star. The source was positioned on the ACIS-S3 CCD with an offset of 40$''$ from the nominal pointing for the S3. The data were collected using a 1/4 subarray mode, which boosted the time resolution to 1.14 s. The CCD temperature was -120°C. Standard pipeline processed level 2 data were used for the analysis. V404 Cyg was clearly detected and the source position is α = 20h 24m 03.82s, δ = +33d 52m 02.14s (J2000), which is in good agreement with the optical and radio position of V404 Cyg (Wagner et al. 1991).

The *Chandra* detectors are known to experience periods of high background, which are particularly significant for the S3 chip (e.g. Garcia et al. 2000). We searched for such background flares in our data by examining the light curve of the entire S3 chip minus the source regions. We found that the background was very stable during the whole observation with an average count rate of 0.13 count s^{-1}. In order to reduce the background, we only analyzed data from 0.3–7 keV. We extracted data from a circle of 3 pixels ($\sim 1.5''$) centered on V404 Cyg and background from an annulus with inner and outer radii of 10 and 50 pixels, respectively. There were 1587 counts in the source region and the expected number of background counts in the source region was only 0.4 counts.

A0620–00 — This source was observed by *Chandra* on 2000 February 29 for 44,000 s. ACIS-S was operated in the standard configuration with a time resolution of 3.24 s. A0620–00 was observed on the S3 chip with a $40''$ offset from the nominal pointing. Background was examined; only intervals where the source-free count rate was less than 0.15 count s^{-1} were selected for analysis. The total net exposure time is 41,189 s. The source position is α = 06h 22m 44.48s, δ = -00d 20m 46.36s (J2000) which is consistent with the optical position (Liu, van Paradijs, & van den Heuvel 2001). The observations cover spectroscopic phases 0.09–1.67 (Orosz et al. 1994; Leibowitz, Hemar, & Orio 1998). Only data from 0.3–7 keV were used for spectral analysis. We extracted data from a circle of $1.86''$ centered on A0620–00. This relatively large aperture encompasses all of the counts in the central region that might reasonably be attributed to the source. There were 137 counts in the source region. The background counts in a $1.86''$ aperture are estimated to be 1.2. This small background level was not subtracted.

GRO J1655–40 — *Chandra* observed GRO J1655–40 on 2000 July 1 for 43,000 s, which corresponds to spectroscopic phases of 0.49–0.68 (van der Hooft et al. 1998). The source was located on ACIS-S3 with $40''$ offset from the aim-point; standard 3.24 s frame transfer time was employed. Good data were selected with background count rate < 0.15 count s^{-1}, resulting in a net exposure of 42,506 s. GRO J1655–40 was very faint; by filtering the data from 0.3–7 keV and applying a circular extraction region of $1.41''$ centered on the source, only 66 counts were collected. This choice of aperture encompasses all of counts in the central region that are attributable to the source. The estimated background counts in a $1.41''$ aperture is estimated to be 0.7; this background was not subtracted. The Chandra source position is α = 16h 54m 00.09s, δ = -39d 50m 45.37s (J2000), which is consistent with the radio and optical position (Hjellming 1994; Bailyn et al. 1995).

XTE J1550–564 — The source was observed on 2000 August 21 for $\sim$ 5,000 s and 2000 September 11 for an additional $\sim$ 5,000 s; the observations cover spectroscopic phases 0.06–0.11 and 0.63–0.68, respectively (Orosz et al. 2001). Technical details of the observations can be found in Tomsick et al. (2001). We used similar procedures to those outlined in Tomsick et al. (2001) to reduce the data. However, we extracted data from 0.3–7 keV and used a smaller circular extraction region with a radius of $2''$, which is sufficient to encompass all of the counts in the central region. There are 66 and 109 counts in the first and the second observations, respectively; we ignored the background counts in the source region, which we estimated to be 0.2 counts for the first observation and 0.3 counts for the second observation .

4. Spectral Analysis

4.1. V404 Cyg

Spectra were extracted with CIAO v2.1 [1] and were analyzed with XSPEC v11 [2] and also SHERPA v2.1.2 [3]. The results from both analysis systems were consistent, and we report the XSPEC results herein. In order to allow χ^2 statistics to be used, all the spectra were grouped into at least 30 counts per spectral bin. Response files were selected according to the CCD temperature with standard CIAO routines. We fit the data with several single-component spectral models including power-law, thermal bremsstrahlung, Raymond-Smith and blackbody models including interstellar absorption. The best-fit parameters determined by these fits are shown in Table 2.

All models except the blackbody model gave statistically acceptable fits to the data ($\chi^2/\nu \lesssim 1$). The power-law model provides the best fit, and yields parameters consistent with previous observations (e.g. $\alpha = 1.81 \pm 0.14$; see Table 1). This best fitting model is shown in Figure 1 and the corresponding plot of confidence regions for column density (N_H) and photon index (α) are shown in Figure 2a. The confidence bounds for the Raymond-Smith model are shown in Figure 2b. The best fit temperature for this model is $kT = 7.5$ keV, and the 90% lower limit on the temperature is $kT > 6.1$ keV.

The hydrogen column density for V404 Cyg from optical observations was estimated to be 5.4×10^{21} cm^{-2} ($A_V = 3.1$; Casares & Charles 1994). The best fit values for N_H from the power law and bremsstrahlung models are marginally higher than the optically determined value, but this does not necessarily argue against these models. X-ray binaries often show absorption in the X-ray flux which is somewhat higher than that determined by their optical absorption (Garcia 1994; Vrtilek et al. 1991).

In order to test if the optically-determined absorption yields an acceptable X-ray spectral fit, we re-ran the fits with the absorption fixed to this value. The results of these fits are also given in Table 2. Even though this N_H value is outside the 99% confidence bounds shown in Figure 2, these fits do yield acceptable values of χ^2/ν (except for the blackbody model). This is a reflection of the fact that the minimum value of χ^2/ν obtained with N_H as a free parameter is slightly less than one, thereby allowing points outside the $\chi^2_{min} + 9.21$ (Lampton, Margon, & Bowyer 1976) contour to have $\chi^2/\nu \sim 1$. For these fits with N_H fixed, the best fit temperature for the Raymond-Smith model is raised to 8.9 keV, and the 90% lower limit is raised to > 7.2 keV.

[1] http://asc.harvard.edu/ciao/

[2] http://heasarc.gsfc.nasa.gov/docs/xanadu/xspec/index.html

[3] http://asc.harvard.edu/ciao/download/doc/sherpa_html_manual/index.html

We do not see any significant Fe-K line emission between 6.4–7 keV, with a 90% confidence upper limit of $\sim$ 800 eV (line width fixed at 0.1 keV) on the equivalent width.

4.2. A0620–00

We analyzed the energy spectrum of A0620–00 using procedures similar to those discussed above for V404 Cyg. We grouped the data into spectral bins containing at least 10 counts and used both χ^2 and CASH (Cash 1979) statistics to estimate the best-fit parameters and their errors. We chose to bin the data in order to achieve enough counts per bin to employ the χ^2 statistic. However, binning the data heavily can result in a loss of spectral information. One can also apply the Gehrels approximation (Gehrels 1986) to permit the use of fewer counts (≤ 5) per bin, but this approach over-estimates the errors. The CASH statistic is a maximum likelihood method designed to estimate the best-fit parameters using unbinned or slightly binned data. This is particularly useful when the source yields only very few photons. The disadvantage of the CASH statistic, relative to the χ^2 statistic, is that it does not provide a goodness-of-fit criterion for comparing different models. It is therefore worthwhile to examine the results obtained using both χ^2 and CASH statistics. In Table 2, except for V404 Cyg, all the best-fit parameters and errors are based on the CASH statistic; the reduced χ^2 values are also shown to indicate the quality of the fit. In order to justify the significance of the CASH statistic, we performed Monte-Carlo simulations to estimate the significant level of the fits; these results are also given in Table 2.

Both methods give very consistent results. We employed the same four single-component models with interstellar absorption that we used for V404 Cyg; the best-fit parameters for the various spectral models are shown in Table 2. Among all the models, the power-law gives the best fit ($\chi^2/\nu = 0.71$, $\alpha = 2.2 \pm 0.5$), while the blackbody gives the worst fit ($\chi^2/\nu = 1.58$); Monte-Carlo simulations based on the CASH statistic also show similar results. The confidence regions for the power-law fit are shown in Figure 2a, and those for the Raymond-Smith fit are shown in Figure 2b. The best fit Raymond-Smith temperature is $kT = 5.5$ keV, and the 90% lower bound on the temperature is $kT > 3.5$ keV.

The values of N_H determined by the power-law and bremsstrahlung fits are consistent with the optical value, corresponding to $N_H = (1.94 \pm 0.28) \times 10^{21}$ cm^{-2} (Wu et al. 1976, 1983; Predehl & Schmitt 1995). The value of N_H determined by the Raymond-Smith and blackbody models is lower than the optical value. This conclusion provides marginal evidence that neither the blackbody nor the Raymond-Smith models are correct descriptions of the source spectrum because X-ray fits tend to find N_H higher than (or consistent with) the optically determined value. As in the case of V404 Cyg, we re-ran the fits with N_H fixed at the optically determined value. The results of these fits are also shown in Table 2. The derived parameters are consistent (within 1σ) with the results obtained by varying N_H, except for the case of the blackbody model. The best-fit temperature for the Raymond-Smith model is 4.1 keV, and the 90% lower bound is > 2.8 keV.

Previously, the best measurement of the X-ray spectrum of A0620–00 was that afforded by *ROSAT* (Narayan et al. 1997a), which gave $\alpha = 3.5 \pm 0.7$ with N_H fixed to the optical value. This led to the speculation that the quiescent X-ray spectra of BHXN with orbital periods $\lesssim 1$ day might be softer than the spectra of longer period systems. However, this result was based on only 39 ± 8 detected source photons in the presence of a significant background. The present result is much more robust because it is based on more than 3 times as many counts, a negligible background, and a much wider energy band. It is important to note that A0620-00 was also a factor of ~ 2 fainter in this *Chandra* observation than it was during the previous *ROSAT* observation. The best fitting power-law model indicates a 0.4–2.4 keV emitted flux of $1.9 \times 10^{-14}\,\mathrm{erg\,cm^{-2}\,s^{-1}}$, corresponding to a luminosity of $2.1 \times 10^{30}\ \mathrm{erg\,s^{-1}}$, which is a factor of two below the *ROSAT* value (see Table 1).

4.3. GRO J1655–40

The spectrum of GRO J1655–40 was analyzed using the same methods discussed above for A0620–00. The energy spectrum was grouped into spectral bins containing at least 5 counts and fit using χ^2 and CASH statistics. Unbinned data was also fit using CASH statistic, and the results were consistent. All simple models give acceptable fits. While the blackbody model gives the poorest fits, it cannot be rejected on the basis of χ^2/ν and Monte-Carlo simulations. However, the N_H for the blackbody model is slightly lower (1.5σ) than the optical value of $(6.66 \pm 0.57) \times 10^{21}$ $\mathrm{cm^{-2}}$ (Predehl & Schmitt 1995; Hynes et al. 1998), while the other three models indicate values of N_H consistent with the optically-derived value. The relatively low value of N_H suggests that the blackbody model may not be a true representation of the source spectrum.

The best fit temperature for the Raymond-Smith model is $kT = 12.24$ keV, and the 90% lower limit on the temperature is $kT > 3.63$. If we fix N_H to the optical value, these values are raised to $kT = 17.15$ keV and $kT > 5.8$ keV.

As above, we list the best fit parameters in Table 2, and show a plot of the confidence regions for power-law and Raymond-Smith fits in Figures 2a and 2b. It is important to note that these observations show GRO J1655–40 to be a factor of ~ 10 fainter than previous quiescent observations (see Table 1). The observed 0.4–2.4 keV emitted flux, for the best fitting power-law model, is $1.5 \times 10^{-14}\ \mathrm{erg\,cm^{-2}\,s^{-1}}$; the observed 0.3–7.0 keV luminosity is $2.4 \times 10^{31}\ \mathrm{erg\,s^{-1}}$. The large decrease in flux and luminosity indicate that the previous *ASCA* observations may not have been taken during the true quiescent state because the observations occurred between two outbursts.

4.4. XTE J1550–564

We combined the two spectra of XTE J1550–564 as shown in Tomsick et al. (2001), grouped the resulting data into bins containing at least 10 counts each, and fit the data to models using χ^2

and CASH statistics. The results of the spectral fits are shown in Table 2, and the corresponding parameter confidence regions are shown in Figure 2. All four models yield statistically acceptable fits, and we see no straightforward way to select one model over the others. With the exception of the blackbody model, all of the models indicate that N_H is somewhat higher than that determined optically (Sánchez-Fernández et al. 1999). However, as indicated above, this is only a weak argument against the blackbody model. Fits with N_H fixed to the optical value are also statistically acceptable, and indicate harder (α lower, kT higher) spectra than the fits with N_H free.

The Raymond-Smith fits indicate a best fit temperature of $kT = 4.38$ keV, and a 90% lower limit to the temperature of $kT > 2.81$ keV. Fits with N_H fixed to the optical value raise these values to $kT = 10.31$ keV and $kT > 5.15$ keV. The results of power-law fit are consistent with those found by Tomsick et al. (2001).

In order to determine if the quiescent X-ray emission of XTE J1550–564 has a flux consistent with a stellar corona, we calculated the unabsorbed X-ray flux (F_X) and bolometric flux for XTE J1550–564 using the methods of Bildsten & Rutledge (2000). Based on our best-fit power-law result, the unabsorbed 0.4–2.4 keV flux of XTE J1550–564 is 2.98×10^{-13} erg cm^{-2} s^{-1}. For the bolometric flux, we used $F_{bol} = 10^{-0.4(V_q+11.51+B.C.-A_V)}$ erg cm^{-2} s^{-1}(Bildsten & Rutledge 2000), where B.C. is the bolometric correction for spectral type, V_q is the quiescent magnitude, and A_V is the reddening. We adopted a V_q of 22 ± 0.2 and a spectral type of K3III from recent VLT observations (Orosz et al. 2001), which indicates B.C.$= -0.8$. We computed F_{bol} using the A_V determined from optical observations ($A_V = 2.17$; Sánchez-Fernández et al. 1999) and find $F_{bol} = 5.1 \times 10^{-13}$ erg cm^{-2} s^{-1}. We also determined F_{bol} using the A_V estimated from our X-ray spectral fitting. For a power-law model, $N_H = 8.73 \times 10^{21}$ cm^{-2} implies that $A_V = 4.88$ (Predehl & Schmitt (1995)], implying $F_{bol} = 6.1 \times 10^{-12}$ erg cm^{-2} s^{-1}. These values of F_{bol} are discussed in Section 6.

5. Time-resolved Spectrum of V404 Cyg

The background-subtracted light curve of V404 Cyg during our observations is shown in Figure 3. The light curve shows a factor of ~ 2 variability in a few ksec. We do not find any significant peak in the power spectrum on timescales from 2.3 s to 10,000 s and the 3σ upper limit on the semi-amplitude is 39% (0.3–7 keV).

The marked variability led us to search for spectral changes at differing flux levels. The data was divided into seven segments based on the source intensity (see Figure 3). The spectrum from each segment contains at least 100 counts. The results of fitting each spectrum with a power-law model are shown in Table 3. The best-fit column density varied between $(2.91 - 11.08) \times 10^{21}$ cm^{-2}, and the best fit photon index α varied between 1.1–2.4. We found no correlation between either the column density or α and the flux. However, we do find a positive correlation between the absorption column and the photon index (see Figure 4) with a correlation coefficient of 0.93 ($>$ 99%).

However, we suspect that this correlation is not intrinsic to the source, but is rather an artifact of the fitting process which links α and N_H. For example, we note that the slope of the correlation is nearly (within $\sim 5\%$) the same as the slope of the major axis of the parameter confidence contours (Figure 2a). Also, we extracted and examined two spectra, one for count rates below 0.11 counts s^{-1} and the other for count rates above 0.18 counts s^{-1} (see Figure 3), and found them to be identical. We conclude that the spectral shape does not vary with intensity.

6. Discussion

We analyzed the *Chandra* ACIS-S X-ray spectra of four BHXN in quiescence by fitting the spectra to simple one component models (power-law, thermal Bremsstrahlung, Raymond-Smith, blackbody) including interstellar absorption. While the statistics afforded by the *Chandra* data surpass that previously available, they are still inadequate to rule out any of these simple model, except for the blackbody model in the case of V404 Cyg. There is some weak additional evidence against a few other models: For A0620–00 the Raymond-Smith and blackbody models imply unlikely values of N_H which are lower than the optically-determined values. The same is true for GRO J1655–40 and XTE J1550–564 in the case of the blackbody model. On the other hand, the thermal bremsstrahlung model provides a good fit to the data in all cases; however, the physical interpretation of this model is unclear (see Christian & Swank 1997). The model which does fit well in all cases and which has a straightforward physical interpretation is the power-law model with a photon index of ~ 2. This slope is consistent with the spectra expected for an ADAF.

Bildsten & Rutledge (2000) suggest that much of the X-ray flux observed from quiescent BHXN may be produced by a rotationally enhanced stellar corona in the secondary star, as seen in tidally-locked binaries such as the RS CVn systems. Lasota (2000) has criticized this view, suggesting instead that the physically smaller secondaries of CVs provide a better analog, and that in this case the expected coronal emission is far below that seen in quiescent BHXN.

The coronal hypothesis of Bildsten & Rutledge (2000) makes two clear, testable predictions. First, that $L_X < 10^{-3} L_{bol}$, and second, that the spectrum of the quiescent BHXN should be similar to that of a stellar corona, i.e., well represented by a Raymond-Smith model with $kT < 1.4$ keV, (Dempsey et al. 1993). The luminosity and spectral evidence available for five of the six BHXN observed by *Chandra* rule strongly against these hypotheses, as detailed below. Note that we do not include in this discussion a seventh BHXN observed with *Chandra* 4U 1543-47, (see G01) because it contains a fully radiative secondary (Orosz et al. 1998) and is not expected to possess an X-ray corona. Consequently, this system is irrelevant to the present discussion.

Figure 5, which is adapted from Bildsten & Rutledge (2000), compares the quiescent fluxes of BHXN with the predictions of the coronal model. The quiescent flux of GRO J0422+32 exceeds the maximum prediction of the coronal model by a factor of ~ 60, and V404 Cyg exceeds this limit by a factor of ~ 40. XTE J1550–564 exceeds the coronal limit by a factor ~ 50 (or ~ 400) for the highest (or lowest) L_{bol} computed in section 4.4. However, the luminosity of XTE J1550–564 should be treated with caution because a mini-outburst occurred 120 d after this observation (see Tomsick et al. 2001). This situation is very similar to the case of the *ASCA* observation of GRO J1655–40 made between two outbursts which gave a high value of the luminosity (see Section 4.3). Finally, A0620–00 is a factor of ~ 5 above the coronal prediction, which may be a significant discrepancy since the prediction corresponds to the maximum likely level of coronal emission.

Turning to the spectral evidence, we find herein that the X-ray spectra of V404 Cyg, A0620-00, GRO J1655–40 and XTE J1550–564 are harder (equivalently hotter) than typical spectra of stellar coronae. The average temperature for these sources as determined from the N_H free (fixed) fits to Raymond-Smith models is 7.4 keV (10.1 keV). The average of the 90% lower limits to the temperatures is > 4 keV (or > 5.24 keV from the N_H fixed fits). Coronal sources are often fit by Raymond-Smith models with two separate temperature components. The average of the higher of these temperatures has a value of 1.4 keV (Dempsey et al. 1993). Thus, in the four systems for which the data are of sufficient quality to allow us to measure the X-ray spectrum, the temperature is ~ 5 to 7 times higher than the higher temperature typically seen from stellar corona.

Thus the combination of spectral and luminosity information argue against a coronal source for the quiescent luminosity in 5 out of the 6 cases for which the coronal mechanism is potentially relevant (i.e. excluding 4U 1543-47). Only in the case of GS 2000+25, where we are unable to determine a spectrum due to the very low number of counts, is it possible that coronal emission from the secondary dominates the quiescent luminosity.

During strong flares, stellar coronae are occasionally seen at temperatures higher than the 1.4 keV average value quoted above. For example, a "super-hot giant flare" from Algol was seen to have a peak temperature of 12.37 keV (Favata & Schmitt 1999). In this regard, it is important to note that both A0620-00 and GRO J1655–40 were observed with *Chandra* at *lower* luminosities than in previous quiescent observations. Therefore it is unlikely that these two systems were in a flaring state during our observations.

Either the secondaries in BHXN have coronae unlike those seen before, or the source of the quiescent luminosity is not coronal. This is not to say that these secondaries do not have X-ray emitting corona, but merely that the luminosity from such a corona is swamped by the accretion luminosity even during quiescence. An obvious point to note is the following. Emission from a stellar corona will contribute at some level to the quiescent X-ray luminosity. If in a few cases this level is significant, then the accretion luminosities of the black holes must be even lower than our estimates and the argument for event horizons would be further strengthened.

It is worth noting that the five BHXN for which coronal emission is ruled out cover the full range of orbital period and stellar bolometric flux. It therefore seems unlikely that there is some particular region of parameter space where the coronal model applies. In comparison, the ADAF model is consistent with all the observations, covering the full parameter space (Narayan et al. 1996, 1997a, 2001; Lasota 2000).

Results of this paper further constrain the required ADAF model. Quataert & Narayan (1999) proposed that significant mass can be lost to an outflow/wind in ADAF models. They also predicted the spectral shape for ADAF models with and without winds for V404 Cyg. Our observations indicate that the power-law photon indices of V404 Cyg, A0620–00, GRO J1655–40 and XTE J1550–564 are consistent with $\alpha \sim 2$. Therefore, models in which Comptonization dominates are favored (Narayan et al. 1997a); strong-wind models become unlikely unless δ (the fraction of the turbulent energy which heats the electrons) is large enough (Quataert & Narayan 1999). ADAF models also predict line emission in X-ray spectra (e.g. Narayan & Raymond 1999). We set an upper limit on the equivalent width of any line feature between 6.4–7 keV for V404 Cyg and it is much higher than the theoretical prediction even for model with winds. A larger collecting area instrument like *XMM-Newton* is needed to study this kind of feature. Recent *RXTE* and *Chandra* observations of XTE J1550–564 also suggest that the ADAF model can explain the quiescent X-ray emission, although it does not explain all the behavior observed at other wavelengths (Tomsick et al. 2001). The similarity of the quiescent spectra of V404 Cyg, XTE J1550–564, GRO J1655–40, and A0620-00 found herein suggests that they may all be described by a similar ADAF model. Detailed broadband spectral modeling of these systems should be considered in order to further constrain the models.

The sources discussed in this paper have a wide range of luminosities. V404 Cyg is the brightest quiescent BHXN in our sample, with a 0.3–7 keV luminosity of $\sim 5 \times 10^{33}$ erg s^{-1}. In our *Chandra* observations the source was somewhat more luminous than in previous quiescent observations in which the luminosity was about 10^{33} erg s^{-1} (see Table 1). Wagner et al. (1994) reported that V404 Cyg exhibited a decrease in intensity by a factor of 10 in < 0.5 day, while our *Chandra* observations showed a factor of 2 variability in a few ksec. Wagner et al. (1994) also found that there may have been a factor ~ 2 variability on timescales of ~ 30 minutes in the highest intensity bins for the *ROSAT* observations. Thus V404 Cyg in quiescence shows variability in X-rays on both short-term (a few ksec) and long-term (years) timescales. Significant X-ray variability in quiescence was also seen in 4U 1630–47 (Parmar et al. 1997), A0620–00 (Asai et al. 1998; Menou et al. 1999; also Table 1) and GX 339–4 (Kong et al. 2000). V404 Cyg and GX 339-4 are similar in some respects: for example, their quiescent X-ray luminosities are comparable (Kong et al. 2000, 2002) and GX 339–4 has also been observed to undergo X-ray variability by a factor of 3 during its quiescent or 'off' state (Kong et al. 2002). Thus, variability in the quiescent state is common, which suggests that BHXN in quiescence are not totally turned off. We note that XTE J1550–564 also varied in luminosity by factor of ~ 2 during the two *Chandra* observations in quiescence (Tomsick et al. 2001); only V404 Cyg and GX 339–4 have a quiescent luminosity higher than XTE J1550–564.

In Figure 6, we plot the Eddington-scaled luminosities (based on the best-fit power-law model) as a function of orbital period P_{orb}; this is an update of the same plot from G01. For the mass of XTE J1550–564 we assumed $M = 10.6 M_{\odot}$ (Orosz et al. 2001); the distance to XTE J1550–564 is estimated to be 2.5–6.3 kpc (e.g. Sánchez-Fernández et al. 1999; Orosz et al. 2001) and we have adopted an average distance of 4 kpc. We note that for the three long orbital period systems (V404 Cyg: 6.47 d, GRO J1655–40: 2.6 d and XTE J1550–564: 1.55 d), the quiescent luminosity is higher than for the other systems (Figure 6). This implies that the accretion rate in these systems is higher than for the others according to the ADAF model (Narayan et al. 1997a; Menou et al. 1999). It is not clear if there is a positive correlation between the luminosities and orbital periods (see Figure 6); a larger sample of long orbital period systems is required to study this correlation.

In summary, we note that our results confirm the prediction of Lasota (2000), who previously pointed out that X-ray emission from a quiescent BHXN is unlikely to come from a stellar coronae; instead he argues that the emission is due to an ADAF. Based on this model, Lasota (2000) predicted fluxes similar to those reported herein. Moreover, he pointed out that detection of GRO J0422+32 by *Chandra* would rule out the coronal model, and such a detection has been made (G01). However, our *Chandra* spectra are able to rule out only a few of the simple, one-component spectral models we fit to the data. With its larger collection area, observations with *XMM-Newton* should be able to do a significantly better job of constraining the source spectra. Additionally, we note that V404 Cyg is variable on a few ksec timescale, so simultaneous optical and X-ray observations may shed substantial light on the quiescent accretion processes in this source.

AKHK was supported by a Croucher Fellowship. JEM was supported in part by NASA grant GO0-1105A. MRG acknowledges the support of NASA LTSA Grant NAG5-10889 and NASA Contract NAS8-39073 to the CXC. The HRC GTO program is supported by NASA Contract NAS-38248.

REFERENCES

Asai, K., Dotani, T., Hoshi, R., Tanaka, Y., Robinson, C.R., & Terada, K. 1998, PASJ, 50, 611

Bailyn, C.D., et al. 1995, Nature, 374, 701

Bildsten, L., & Rutledge, R.E. 2000, ApJ, 541, 908

Callanan, P.J., Charles, P.A., Honey, W.B., & Thorstensen, J.R. 1992, MNRAS, 259, 395

Campana, S., Parmar, A.N., & Stella, L. 2001, A&A, 372, 241

Casares, J., & Charles, P.A. 1994, MNRAS, 271, L5

Cash, W. 1979, ApJ, 228, 939

Christian, D.J., & Swank, J.H. 1997, ApJS, 109, 177

Dempsey, R.C., Linsky, J.L., Schmitt, J.H.M.M., & Fleming, T.A. 1993, ApJ, 413, 333

Favata, F., & Schmitt J.H.M.M. 1999, A&A, 350, 900

Garcia, M.R., McClintock, J.E., Narayan, R., Callanan, P., Barret, D., & Murray, S.S., 2001, 553, L47 (G01)

Garcia, M.R., Murray, S.S., Primini, F.A., Forman, W., McClintock, J.E., & Jones, C. 2000, ApJ, 537, L23

Garcia, M.R. 1994, ApJ 435, 407

Gehrels, N. 1986, ApJ, 303, 336

Hjellming, R.M. 1994, IAUC 6055

Hynes, R.I., Haswell, C.A., Shrader, C.R., Chen, W., Horne, K, Harlaftis, E.T., O'Brien, K., Hellier, C., & Fender, R.P. 1998, MNRAS, 300, 64

Kong, A.K.H., Kuulkers, E., Charles, P.A., & Homer, L. 2000, MNRAS, 312, L49

Kong, A.K.H., Charles, P.A., Kuulkers, E., & Kitamoto, S. 2002, MNRAS, 329, 588

Lampton, M., Margon, B., & Bowyer, S. 1976 ApJ 208, 177

Lasota, J.-P. 2000, A&A, 360, 575

Leibowitz, E.M., Hemar, S., & Orio, M. 1998, MNRAS, 300, 463

Liu, Q.Z., van Paradijs, J., & van den Heuvel, E.P.J. 2001, A&A, 368, 1021

McClintock, J.E., Horne, K., & Remillard, R.A. 1995, ApJ, 442, 358

Menou, K., Esin, A.A., Narayan, R., Garcia, M.R., Lasota, J.-P., & McClintock, J.E. 1999, ApJ, 520, 276

Narayan, R., McClintock, J.E., & Yi, I. 1996, ApJ, 457, 821

Narayan, R., Barret, D., & McClintock, J.E. 1997a, ApJ, 482, 448

Narayan, R., Garcia, M.R., & McClintock, J.E. 1997b, ApJ, 478, L79

Narayan, R., Garcia, M.R., & McClintock, J.E. 2001, to appear in Proc. IX Marcel Grossmann Meeting, eds. V. Gurzadyan, R. Jantzen and R. Ruffini, Singapore: World Scientific

Narayan, R., & Raymond, J. 1999, ApJ, 515, L69

Orosz, J.A., Bailyn, C.D., Remillard, R.A., McClintock, J.E., & Foltz, C.B. 1994, ApJ, 436, 848

Orosz, J.A., Jain, R.K., Bailyn, C.D., McClintock, J.E., & Remillard, R.A. 1998, ApJ, 499, 375

Orosz, J.A., Groot, P.J., van der Klis, M., McClintock, J.E., Garcia M.R., Zhao P., Jain R.K., Bailyn C.D., & Remillard R.A. 2001, ApJ, in press (astro-ph/0112101)

Parmar, A.N., William, O.R., Kuulkers, E., Angelini, L., & White, N.E. 1997, A&A, 319, 855

Predehl, P., & Schmitt, J.H.M.M. 1995, A&A, 293, 889

Quataert, E., & Narayan, R. 1999, ApJ, 520, 298

S*á*nchez-Fern*á*ndez, et al. 1999, A&A, 348, L9

Tanaka, Y., & Lewin, W.H.G. 1995, in X-ray Binaries, p.126, eds Lewin, W.H.G., van Paradijs J., ban den Heuvel, E.P.J., Cambridge Univ. Press, Cambridge.

Tanaka, Y., & Shibazaki, N. 1996, ARAA, 34, 607

Tomsick, J.A., Corbel, S., & Kaaret, P. 2001, ApJ, 563, 229

Ueda, Y., Inoue, H., Tanaka, Y., Ebisawa, K., Nagase, F., Kotani, T., & Gehrels, H. 1997, ApJ, 492, 782

van der Hooft, F., Heemakerk, M.H.M., Alberts, F., & van Paradijs, J. 1998, A&A, 329, 538

van Paradijs, J., & McClintock, J.E. 1995, in X-ray Binaries, p.58, eds Lewin, W.H.G., van Paradijs J., van den Heuvel, E.P.J., Cambridge Univ. Press, Cambridge.

Vrtilek, S.D., McClintock, J.E., Seward, F.D., Kahn, S.M., & Wargelin, B.J. 1991, ApJS, 76, 1127

Wagner, R.M., Starrfield, S.G., Hjellming, R.M., Howell, S.B., & Kreidl, T.J. 1994, ApJ, 429, L25

Wagner, R.M., Bertram, R., Starrfield, S.G., Howell, S.B., Kreidl, T.J., Bus, S.J., Cassatella, A., & Fried, R. 1991, ApJ, 378, 293

Wu, C.-C., Aalders, J.W.G., van Duinen, R.J., Kester, D., & Wesselius, P.R. 1976, A&A, 50, 445

Wu, C.-C., Panek, R.J., Holm, A.V., Schmitz, M., & Swank, J.H. 1983, PASP, 95, 391

This preprint was prepared with the AAS LATEX macros v5.0.

TABLE 1
PREVIOUS QUIESCENT OBSERVATIONS OF BLACK HOLE X-RAY NOVAE

Source	Date	Instrument	N_H (10^{22} cm^{-2})	α	Luminosity (10^{33} erg s^{-1})	Distance (kpc)	References
V404 Cyg	1992 Nov	*ROSAT*	2.29^{a}	$6^{\dagger}$	8.1 (0.1–2.4 keV)	3.5	1
			2.1^{a}	$4.0^{+1.9}_{-1.5}$	1.1 (0.7–2.4 keV)		2
	1994 May	*ASCA*	$1.1^{+0.3}_{-0.4}$	$2.1^{+0.5}_{-0.3}$	1.20 (1–10 keV)		3
	1996 Sept	*BeppoSAX*	1.0 (fixed)	$1.9^{+0.6}_{-0.3}$	1.04 (1–10 keV)		4
A0620–00	1992 Mar	*ROSAT*	0.16 (fixed)	$3.5^{+0.8}_{-0.7}$	0.004 (0.4–1.4 keV)	1.0	2
	1994 Mar	*ASCA*	1.6 (fixed)	2 (fixed)	< 0.008 (0.5–10 keV)		5
GRO J1655–40	1996 Mar	*ASCA*	< 0.3	$0.7^{+2.1}_{-0.4}$	0.3 (0.5–10 keV)	3.2	5
XTE J1550–564	2000 Aug & Sep	*Chandra*	$0.85^{+2.2}_{-2.4}$	2.3 ± 0.4	0.67 (0.5–7 keV)	2.5–6.3	6,7

NOTES — † Uncertainty not given. For XTE J1550–564, the luminosity is based on a distance of 4 kpc.

(1) Wagner et al. 1994; (2) Narayan et al. 1996; (3) Narayan et al. 1997a; (4) Campana et al. 2001; (5) Asai et al. 1998; (6) Tomsick et al. 2001; (7) Orosz et al. 2001

TABLE 2

BEST-FITTING SPECTRAL PARAMETERS

Source	Model	N_H (10^{21} cm^{-2})	α	kT/kT_{RS} [a] (keV)	χ^2_ν/dof (prob)	CASH M-C Prob[b]	Flux[c]
V404 Cyg	Power-law	6.98 ± 0.76	1.81 ± 0.14		0.92/45 (0.63)		1.42
	Bremsstrahlung	$6.04^{+0.60}_{-0.55}$		$6.68^{+2.49}_{-1.50}$	0.94/45 (0.57)		1.40
	Raymond-Smith	$5.82^{+0.56}_{-0.50}$		$7.54^{+2.70}_{-1.43}$	1.11/45 (0.28)		1.57
	Blackbody	2.30 ± 0.42		0.81 ± 0.04	2.09/45 (0.00002)		1.26
	Power-law	5.40 (fixed)	1.55 ± 0.07		1.20/46 (0.17)		1.47
	Bremsstrahlung	5.40 (fixed)		8.66 ± 2.13	1.0/46 (0.46)		1.42
	Raymond-Smith	5.40 (fixed)		8.89 ± 1.57	1.13/46 (0.25)		1.57
	Blackbody	5.40 (fixed)		0.69 ± 0.03	3.49/46 (10^{-14})		1.15
A0620–00	Power-law	$2.37^{+1.14}_{-1.04}$	2.19 ± 0.50		0.71/11 (0.73)	0.78	0.018
	Bremsstrahlung	$1.52^{+0.72}_{-0.67}$		$3.11^{+3.59}_{-1.17}$	0.75/11 (0.69)	0.74	0.018
	Raymond-Smith	$1.05^{+0.57}_{-0.50}$		$5.46^{+6.51}_{-2.07}$	1.03/11 (0.42)	0.48	0.022
	Blackbody	0 [d]		$0.57^{+0.06}_{-0.07}$	1.58/11 (0.10)	0.10	0.017
	Power-law	1.94 ± 0.28 (fixed)	$2.07^{+0.28}_{-0.19}$		0.71/12 (0.74)	0.75	0.018
	Bremsstrahlung	1.94 ± 0.28 (fixed)		$2.55^{+1.44}_{-0.73}$	0.78/12 (0.67)	0.68	0.016
	Raymond-Smith	1.94 ± 0.28 (fixed)		$4.15^{+2.66}_{-1.30}$	1.38/12 (0.17)	0.14	0.023
	Blackbody	1.94 ± 0.28 (fixed)		0.30 ± 0.03	2.39/12 (0.004)	0.00	0.009
GRO J1655–40	Power-law	$8.59^{+6.19}_{-4.52}$	$1.70^{+0.88}_{-0.78}$		0.83/9 (0.59)	0.66	0.017
	Bremsstrahlung	$7.72^{+5.11}_{-3.46}$		$8.40^{+\infty}_{-5.73}$	0.83/9 (0.58)	0.66	0.016
	Raymond-Smith	$7.18^{+4.23}_{-2.97}$		$12.24^{+\infty}_{-8.61}$	0.85/9 (0.56)	0.63	0.019
	Blackbody	$3.03^{+3.47}_{-2.13}$		$0.88^{+0.29}_{-0.18}$	0.94/9 (0.49)	0.57	0.012
	Power-law	6.66 ± 0.57 (fixed)	1.47 ± 0.40		0.75/10 (0.67)	0.60	0.016
	Bremsstrahlung	6.66 ± 0.57 (fixed)		$13.21^{+\infty}_{-8.98}$	0.75/10 (0.68)	0.64	0.015
	Raymond-Smith	6.66 ± 0.57 (fixed)		$17.15^{+\infty}_{-11.35}$	0.77 /10 (0.65)	0.62	0.018
	Blackbody	6.66 ± 0.57 (fixed)		$0.76^{+0.14}_{-0.12}$	1.07/10 (0.38)	0.39	0.012
XTE J1550–564	Power-law	$8.73^{+2.42}_{-2.93}$	$2.28^{+0.47}_{-0.64}$		1.27/13 (0.22)	0.22	0.16
	Bremsstrahlung	$6.93^{+2.13}_{-1.85}$		$3.36^{+4.75}_{-1.33}$	1.26/13 (0.23)	0.24	0.15
	Raymond-Smith	$6.50^{+1.97}_{-1.62}$		$4.38^{+4.31}_{-1.57}$	1.22/13 (0.25)	0.21	0.18
	Blackbody	$3.04^{+1.80}_{-1.49}$		$0.69^{+0.11}_{-0.09}$	1.39/13 (0.16)	0.18	0.14
	Power-law	3.90 ± 0.60 (fixed)	1.35 ± 0.25		1.68/14 (0.05)	0.02	0.17
	Bremsstrahlung	3.90 ± 0.60 (fixed)		$12.56^{+\infty}_{-7.18}$	1.59/14 (0.07)	0.04	0.15
	Raymond-Smith	3.90 ± 0.60 (fixed)		$10.31^{+\infty}_{-5.16}$	1.61/14 (0.07)	0.03	0.16
	Blackbody	3.90 ± 0.60 (fixed)		$0.65^{+0.08}_{-0.06}$	1.39/14 (0.15)	0.15	0.12

NOTES — All quoted uncertainties are 90% confidence.

Except for V404 Cyg, the best-fit parameters and uncertainties are based on the CASH statistic. The reduced χ^2 values were obtained in a separate analysis using the χ^2 statistic.

[a] Thermal bremsstrahlung, blackbody or Raymond-Smith temperature (solar abundance)

[b] For A0620–00, GRO J1655–40, and XTE J1550–564, we list one minus the probability that the best fit model would produce a lower value of the CASH statistic than that calculated from the data, as determined via XSPEC Monte-Carlo simulations. A low probability indicates a poor fit.

[c] Absorbed flux in 0.3–7 keV (10^{-12} erg cm^{-2} s^{-1})

[d] N_H hit the minimum value of 0 allowed by XSPEC

TABLE 3

TIME-RESOLVED SPECTRAL PARAMETERS

	N_H (10^{21} cm^{-2})	α	χ^2_ν/dof	Luminosity[a]
1	10.21 ± 2.28	2.41 ± 0.41	1.21/11	8.07
2	5.08 ± 1.19	1.57 ± 0.26	0.88/16	2.81
3	6.14 ± 1.97	1.72 ± 0.40	0.41/7	4.83
4	6.47 ± 1.09	1.60 ± 0.20	0.85/28	2.81
5	2.91 ± 1.29	1.14 ± 0.40	1.17/6	4.26
6	5.86 ± 1.18	1.56 ± 0.24	0.85/21	3.82
7	11.08 ± 2.15	2.22 ± 0.31	1.11/17	5.32

NOTES — [a] Luminosity in 0.3–7 keV (10^{33} erg s^{-1}), assuming a distance of 3.5 kpc

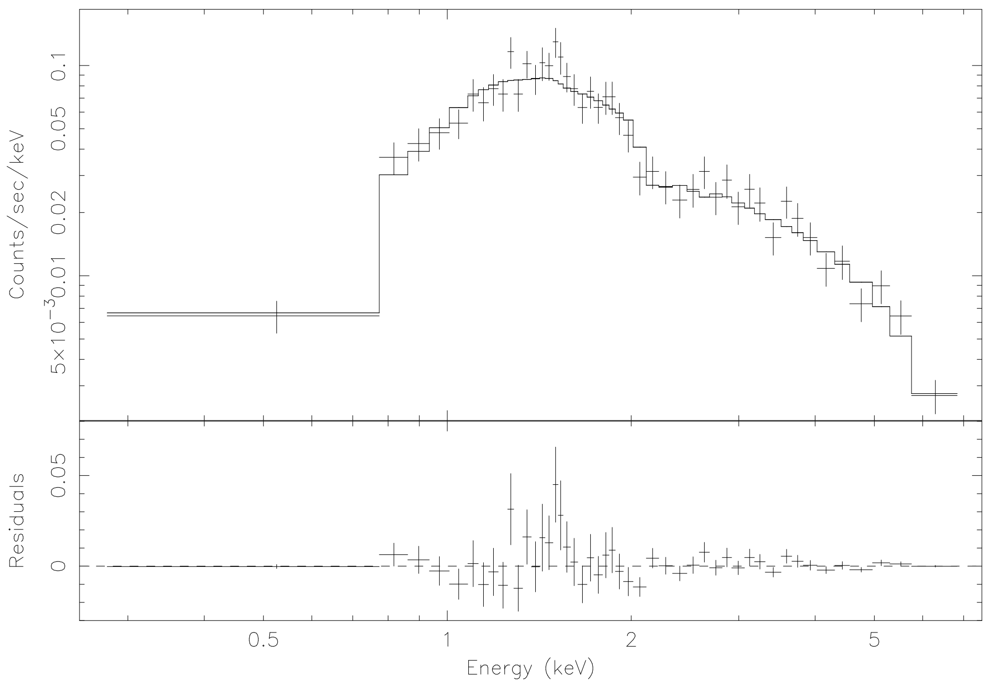

Fig. 1.— Upper panel: The *Chandra* spectrum of V404 Cyg with an absorbed power-law model ($\alpha = 1.81$ and $N_H = 6.98 \times 10^{21}$ cm^{-2}). Lower panel: residuals after subtracting the fit from the data in units of 1σ.

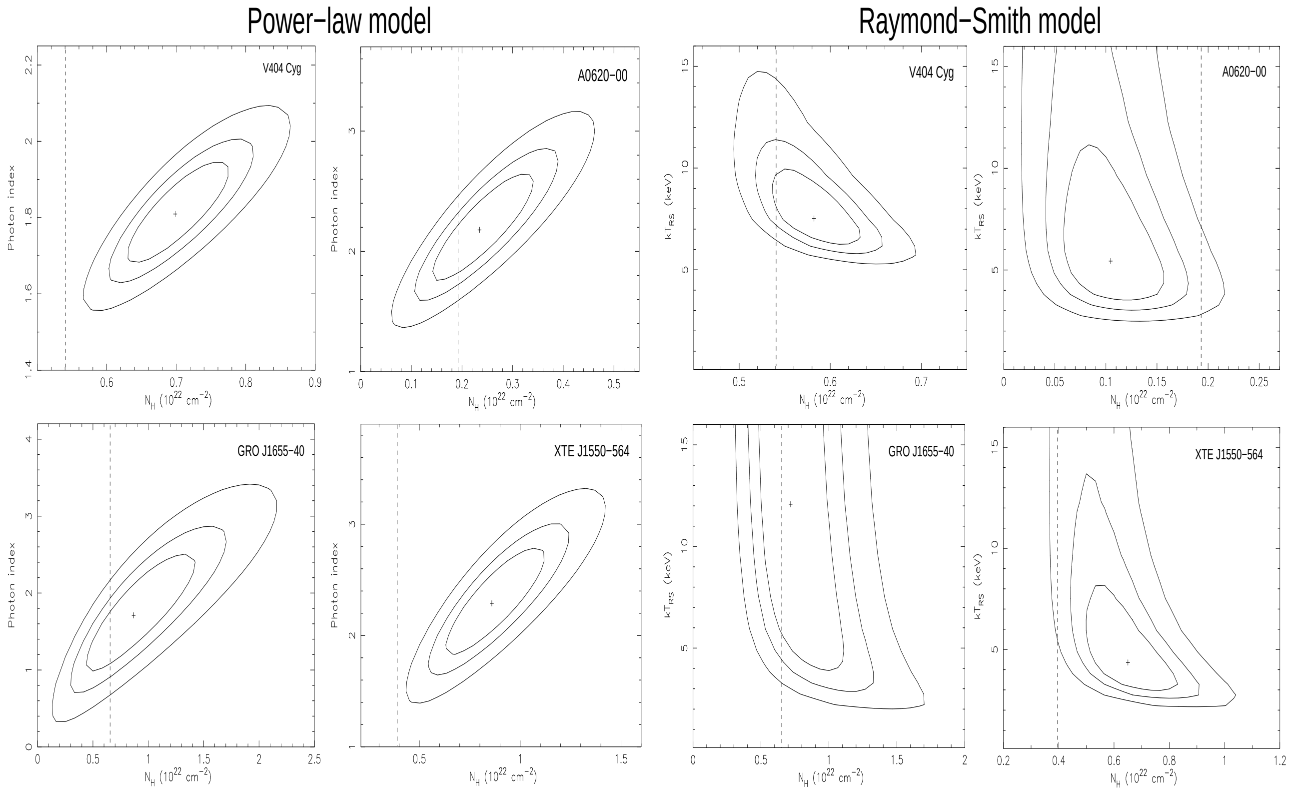

Fig. 2.— Left: Contour plot for the column density (N_H) and photon index (α) derived from the *Chandra* spectrum of V404 Cyg, A0620–00, GRO J1655–40 and XTE J1550–564. The cross in the center marks the best fit parameters and the contours encompass the 68%, 90% and 99% confidence levels. Vertical dashed lines show the optically determined N_H. Right: Contour plot for the column density (N_H) and Raymond-Smith temperature (kT_{RS}) derived from the *Chandra* spectrum of V404 Cyg, A0620–00, GRO J1655–40 and XTE J1550–564. The cross in the center marks the best fit parameters and the contours encompass the 68%, 90% and 99% confidence levels. Except for V404 Cyg, all of the plots were derived using CASH statistic. Vertical dashed lines show the optically determined N_H.

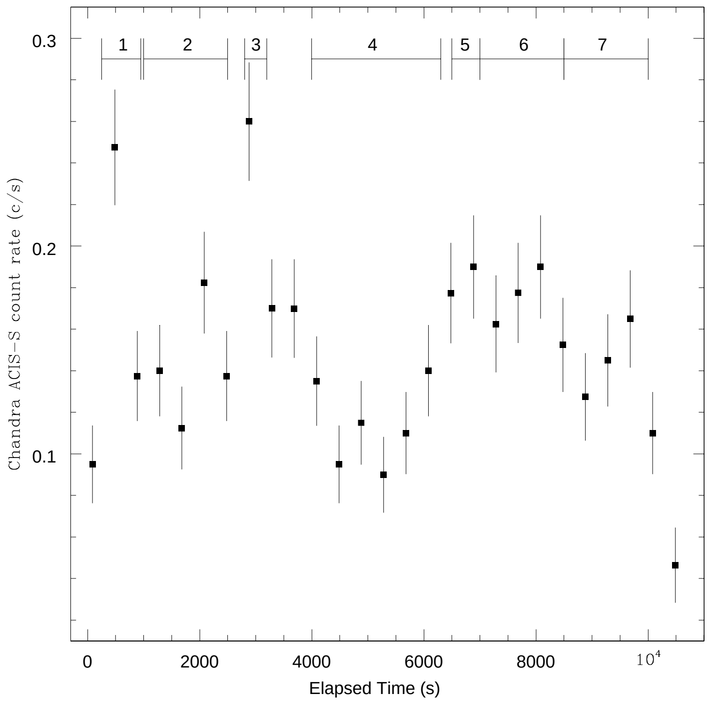

Fig. 3.— *Chandra* ACIS-S 10 ksec light curve of V404 Cyg in the 0.3–7.0 keV band. The time resolution is 500 s. Also shown are the seven time intervals used for time-resolved spectral analysis.

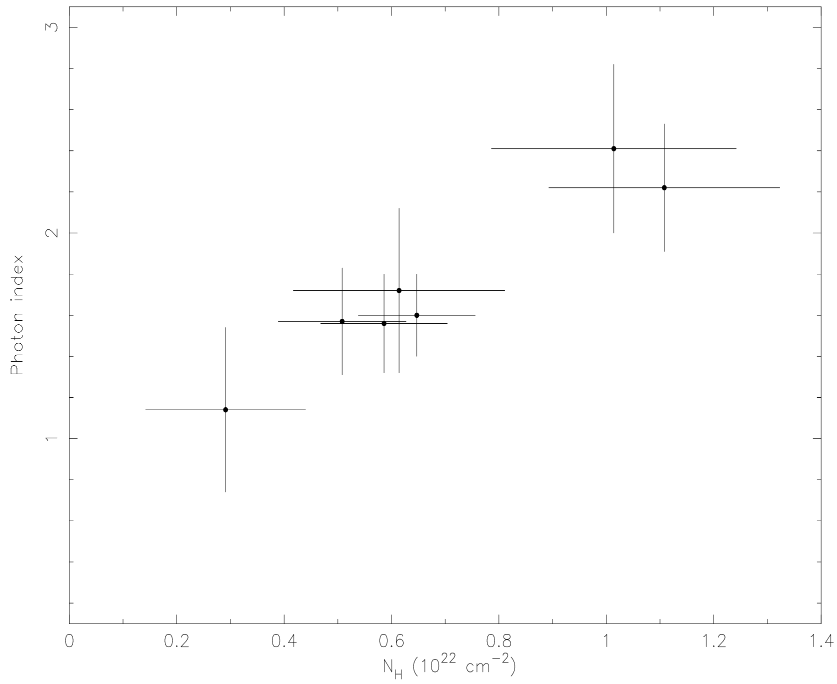

Fig. 4.— Plot of power-law photon index (α) against absorption column density (N_H). A positive correlation can be seen.

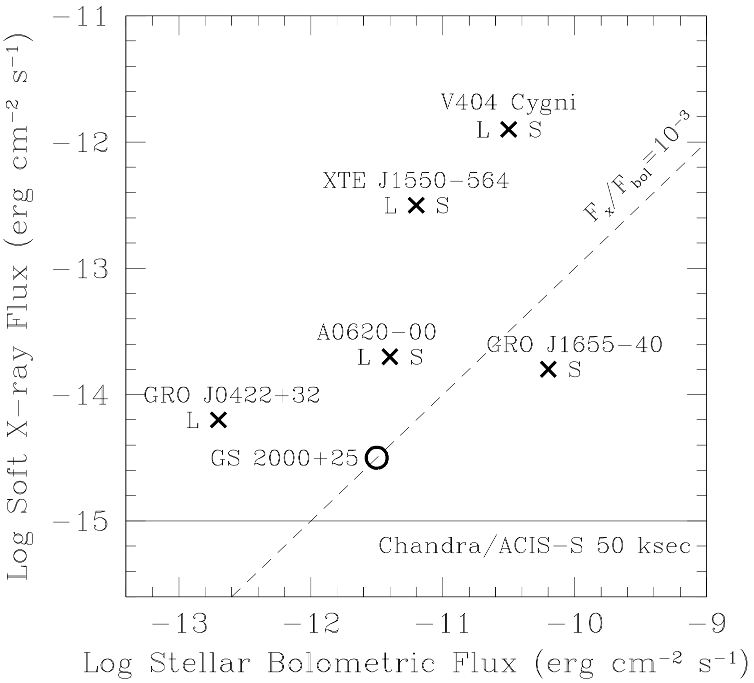

Fig. 5.— Quiescent X-ray and Bolometric Fluxes of BHXN, after Bildsten & Rutledge (2000). X-ray fluxes are as reported herein or from G01, but in all cases converted to 0.4–2.4 keV emitted fluxes (note that Figure 2 of Narayan, Garcia and McClintock (2001) plotted a 0.5–10.0 keV flux for V404 Cyg but agrees with this plot in all other respects). In cases where the spectrum cannot be determined, we have assumed $\alpha = 2$. Bolometric fluxes are from Bildsten & Rutledge (2000) or as reported herein. An "X" indicates that the X-ray flux is unlikely to be due to a stellar corona, An L (S) indicates that it is the X-ray luminosity (spectrum) that argues against this coronal hypothesis. Based on the data herein, in only one (GS 2000+25) of the six BHXN studied could the corona of the secondary produce a signficant part of the detected X-ray flux.

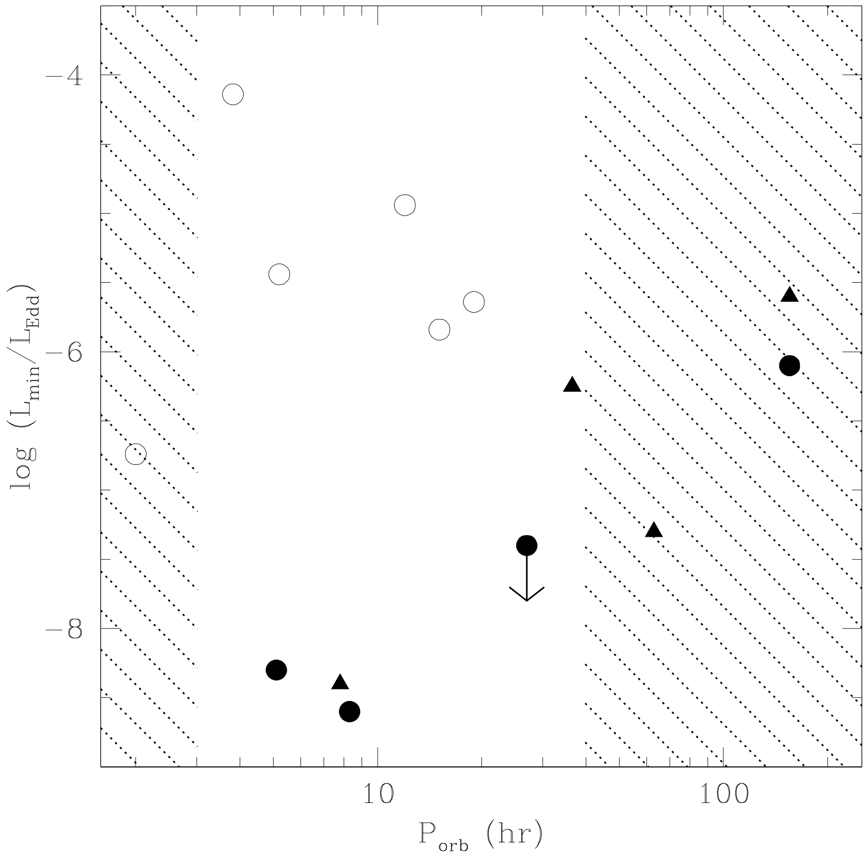

Fig. 6.— Quiescent luminosities of BHXN (filled circles and triangles) and NSXN (open circles) after G01. Data points in triangle are from the results of this work. Only the lowest quiescent detections (except for V404 Cyg which we show both the lowest detection and the luminosity derived here) or *Chandra* upper limits are shown. The non-hashed areas represent common orbital periods for BH and NSXN. The BHXN shown are, from left to right: GRO J0422+32, A0620–00, GS 2000+25, 4U 1543–47, XTE J1550–564, GRO J1655–40 and V404 Cyg.